



# Blueschist-facies paleo-earthquakes in a serpentinite channel (Zagros suture, Iran) enlighten seismogenesis in Mariana-type subduction margins



Jesús Muñoz-Montecinos<sup>a,b,\*</sup>, Samuel Angiboust<sup>a</sup>, Antonio Garcia-Casco<sup>b,c</sup>

<sup>a</sup> Université de Paris, Institut de physique du globe de Paris, CNRS, F-75005 Paris, France

<sup>b</sup> Department of Mineralogy and Petrology, Faculty of Sciences, University of Granada, Campus Fuentenueva s/n, 18002 Granada, Spain

<sup>c</sup> Instituto Andaluz de Ciencias de la Tierra, CSIC-Universidad de Granada, 18100 Armilla, Granada, Spain

## ARTICLE INFO

### Article history:

Received 19 November 2020

Received in revised form 10 July 2021

Accepted 27 July 2021

Available online 18 August 2021

Editor: A. Webb

### Keywords:

Mariana-type margins

blueschists

earthquakes

paleo-earthquakes

ultracataclasites

Zagros suture

## ABSTRACT

The architecture and pressure-temperature conditions reached by a Cretaceous block-in-matrix serpentinite mélangé exposed in the Zagros suture resemble those imaged in the active Mariana subduction zone. There, large magnitude-earthquakes ( $M_w > 9$ ) have never been recorded but smaller events – of poorly-constrained physical origin – in the range  $M_w \sim 3-6$  are widespread. Field and petro-structural constraints led to a first report of blueschist-facies seismic fault-related rocks in the Zagros serpentinite melange, including breccias, foliated cataclasites and ultracataclasites; all observed within a foliated mafic metatuffaceous block embedded in serpentinite schists. Fine-scale petrological characterization of ultrafine-grained, fluidized cataclastic material reveals the presence of newly-formed glaucophane, lawsonite, phengite, albite and pumpellyite, an assemblage inferred (based on thermodynamic modelling) to have crystallized in the lower lawsonite-blueschist facies at  $\sim 0.6-1.0$  GPa and  $230-300$  °C. Extensional veins containing similar mineral assemblages are observed crosscutting the aforementioned rocks but are also identified as comminuted fragments in all fault-related lithologies. Crosscutting relationships among the multiple generations of fluidized ultracataclasites and brecciated blueschists suggest that episodic faulting and hydrofracturing were contemporaneous processes at  $\sim 20-35$  km depth, i.e., at similar conditions as reported for metabasalts expelled by Mariana serpentinite mud volcanoes. Mechanical modelling confirms that the studied fault-related features can only have formed under nearly lithostatic pore fluid pressure conditions, maintaining the system in a critically unstable regime that promoted recurrent seismic faulting, as monitored in the Mariana seismogenic zone. These fluids are likely associated with externally and deeply-generated fluid pulses that may have reached the seismogenic window, imprinting a Ta-Th-Nb-HREEs-enriched trace element signature. This new faulted blueschist occurrence highlights the physical nature and the mechanical processes operating within fluid-saturated fault zones in the serpentinitized subduction channel.

© 2021 The Author(s). Published by Elsevier B.V. This is an open access article under the CC BY license (<http://creativecommons.org/licenses/by/4.0/>).

## 1. Introduction

Mariana-type subduction settings are believed to represent the “aseismic”, non-accretionary end-member where moderate-magnitude seismicity is widespread but no large megathrust earthquakes ( $M_w > 9.0$ ) are so far reported (e.g. Emry et al., 2011 and references therein). This absence was explained by Hyndman et al. (1997) who suggested that a highly serpentinitized mantle – thought to promote aseismic creep – intersects the plate inter-

face at shallow depths inhibiting earthquake nucleation. Recently, Emry et al. (2011) and Eimer et al. (2020) challenged this hypothesis demonstrating that the seismogenic region of the Mariana subduction zone spans the depth range 10 to 60 km along a highly serpentinitized region of the plate interface (Fryer et al., 2020), demonstrating that brittle deformation is actively occurring there. Emry et al. (2011) emphasized that the lack of large earthquakes along the Mariana margin is produced by frictional strength heterogeneities of the megathrust possibly associated with subducting roughness, fluid overpressuring and serpentinitization of the forearc mantle. In addition to moderate magnitude megathrust earthquakes, extensional seismicity is commonly observed in the outer rise region in the vicinity of the trench (Eimer et al., 2020)

\* Corresponding author.

E-mail addresses: [jmunoz@correo.ugr.es](mailto:jmunoz@correo.ugr.es) (J. Muñoz-Montecinos), [angiboust@ipgp.fr](mailto:angiboust@ipgp.fr) (S. Angiboust), [agcasco@ugr.es](mailto:agcasco@ugr.es) (A. Garcia-Casco).

or as tensional normal-faulting in the subducting slab (Emry et al., 2011), possibly associated with gravitational slab pull and roll-back.

On a petrological perspective, rock fragments dredged from serpentinite mud volcanoes in the Mariana forearc preserve mineral paragenesis indicating lower blueschist-facies metamorphism (~150–250 °C at 0.5–0.6 GPa; Maekawa et al., 1993). Recent discoveries demonstrate that some of the blueschist fragments may have been buried to greater depths of ~50 km (590 °C at 1.6 GPa) before being exhumed (Tamblyn et al., 2019). These rock clasts were brought back to the surface through channel flow and serpentinite mud volcanism which is thought to be triggered by slab devolatilization and subsequent fluid flow along normal faults in the forearc (Fryer et al., 2020). These observations suggest that the Mariana forearc is extensively serpentinitized and the ascent of fluidized serpentinite material (protrusion) and rare blueschist fragments is due to diapiric buoyancy forces associated with deep return flow in an extensional regime (Maekawa et al., 2004). On-land fossilized analogues to Mariana-type serpentinite channel are exceptionally preserved in HP-LT suture zones where “mélanges” exhibit blueschist-facies metavolcanic (and metasedimentary) blocks wrapped by a serpentinite matrix. Some key localities correspond to the Franciscan complex (California, United States; Cloos, 1986; Grove and Bebout, 1995), the Kamuikotan belt (Hokkaido, Japan; Maekawa et al., 2004) and the herein studied Seghin complex (Soghan region, Iran; Muñoz-Montecinos et al., 2021).

Although most of the worldwide observed earthquake activity is reported in subduction zones (e.g., Scholz and Campos, 2012), evidence for localized slip at seismic rates from exhumed high pressure-low temperature (HP-LT) metamorphic complexes is extremely scarce (e.g., Austrheim and Andersen, 2004; John and Schenk, 2006). In the blueschist-facies, it is expected that the mechanical behaviour of the subducting slab is transitional between conditionally stable aseismic creep and unstable stick-slip faulting (Austrheim and Andersen, 2004; Behr and Platt, 2013; Angiboust et al., 2015). Evidence for seismic faulting includes the formation of pseudotachylytes and/or fault gouges which are commonly found in dry crystalline rocks (Sibson and Toy, 2006; Bonnet et al., 2019). Recent studies arguing for pseudotachylyte formation in water-saturated fault zones demonstrate the presence of fluids during frictional melting/sliding processes (Meneghini et al., 2010; Menant et al., 2018), but the fluid-rock mechanical feedbacks during seismic slip remain to be better documented (Rowe et al., 2005; Di Toro et al., 2009; Fagereng et al., 2018). Even if elevated pore fluid pressures reduce the effective normal stresses promoting brittle faulting and inhibiting the formation of frictional melts (thermal pressurization and lubrication; Rice, 2006; Di Toro et al., 2009), the low shear stresses expected in subduction settings (e.g., Dielforder et al., 2020) suggest that the occurrence of fluidized fault gouges (e.g., fluidized ultracataclasites) are likely more representative of earthquakes in these environments (e.g., Ujiie et al., 2007; Meneghini et al., 2010).

We herein present a first report of fluidized fault rocks (cataclasites and ultracataclasites) interpreted to represent blueschist-facies paleo-earthquakes in mafic blueschists discovered in the Zagros suture (Seghin complex); a HP-LT mélange composed of blueschist blocks wrapped by a serpentinite matrix which presumably formed in a Mariana-type paleo-subduction margin (Muñoz-Montecinos et al., 2021). This work addresses water-saturated frictional sliding processes combining petro-structural observations with mechanical modelling and compares the observed structural features with what is currently being imaged and dredged in the active Mariana subduction margin.

## 2. Geological context of the Seghin complex

### 2.1. Regional background

The Soghan region exhibits the unique HP-LT remnants of the paleosubduction zone between Eurasia and Arabia plates (Lower Cretaceous-Eocene) exposed now in the Zagros suture (Fig. 1A; Delaloye and Desmons, 1980; Agard et al., 2006 and references therein). In this region, the uppermost Ashin complex represents a paleo-accretionary system (comprising ultramafic domains) metamorphosed at amphibolite-facies conditions during middle Cretaceous times, followed by blueschist-facies overprinting (Angiboust et al., 2016). While the lowermost Siah-Kuh massif has been characterized as a former seamount subducted down to lower blueschist-facies conditions during Upper Cretaceous times (Bonnet et al., 2019, 2020). We focus here on the Seghin complex (Fig. 1B), a km-thick tectonic sliver structurally sandwiched between the Ashin and Siah-Kuh complexes, composed of blueschist blocks embedded in a serpentinite matrix. Peak metamorphic conditions of 1.5–1.8 GPa (~430–530 °C; Fig. 1C) at ~62–75 Ma are recorded by some of the mafic blocks (Sabzehei, 1974; Angiboust et al., 2016). Overall, petrological investigations demonstrate that the tectonic slices exposed in the Soghan region record contrasted P-T-time metamorphic paths documenting the cooling of the subduction thermal gradient from ~17 down to 7 °C/km from ~95 to 65 Ma (Angiboust et al., 2016; Fig. 1C).

### 2.2. Geology of the Seghin complex

The Seghin complex is composed of a moderately dipping antigorite-rich ultramafic schistose matrix wrapping stiffer, metre to hectometre-sized, blueschist tuffaceous blocks showing a sub-vertical main foliation striking ENE-NE (Fig. 1B; see also Sabzehei, 1974). In the serpentinites, no remnant of the ultramafic protolith is observed while the lithological contacts with the blueschist blocks are generally sharp and devoid of blackwall rinds. The blueschist blocks are mainly fine-grained glaucophane-, lawsonite- and jadeitic-omphacitic clinopyroxene-bearing rocks (Angiboust et al., 2016). The same index phases are present in prograde, centimetre-wide metamorphic veins that follow or crosscut the main foliation, while aragonite occurs as vein-filling material in hydraulic breccias. It is worth mentioning that these veins are highly strained due to burial-related shearing according to the main foliation (Muñoz-Montecinos et al., 2021). Minor metasedimentary material is present as isolated blocks or interlayered within blueschists, mostly in the basal part of the Seghin complex.

## 3. Field observations on fault-related rocks

In the studied area (Fig. 1A), an elongated block of blueschist occurs in direct and sharp contact with the surrounding antigorite schist matrix (Fig. 2A and B). The latter also enclosing further dismembered blueschist fragments and showing cataclastic fabrics such as reworked serpentinite and vein fragments in the foliated serpentinite matrix (Fig. S1A). These brittle networks are difficult to follow at several metres scale, due to the strong weathering of the soft serpentinite. A brittle fault zone (up to 4 m-wide but variable along strike) crosscuts at high angle the studied well-foliated hectometre-sized blueschist block from the mélange (Fig. 2A, C and S1B). In the damage zone of this fault network, the most common lithology is a chaotic blueschist breccia including unsorted, up to tens of centimetre-wide angular to rounded blueschist and vein fragments enclosed in a very fine-grained foliated cataclastic matrix (Fig. 2D and E). A precise localization of the fault core was not possible. Brittle deformation was accompanied by extensive

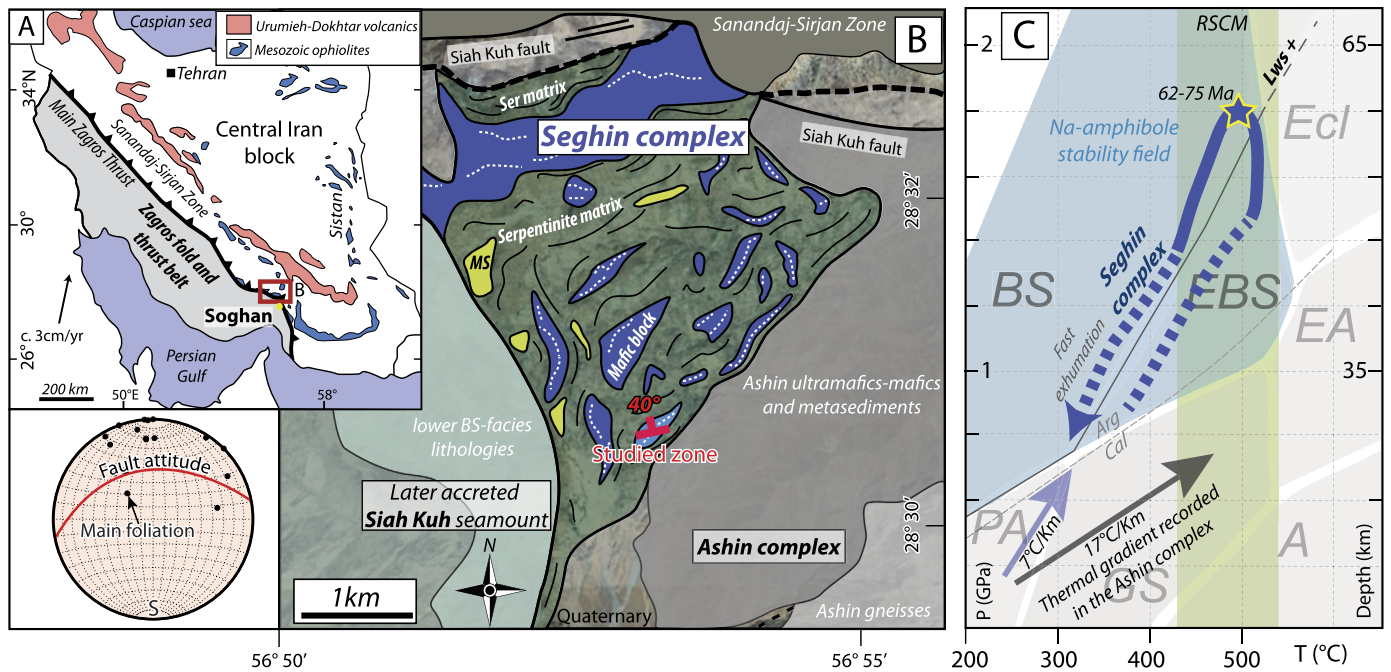


**Fig. 1.** A. Regional geological map of southeastern Iran showing major geological features (modified from Angiboust et al., 2016). B. Local geological map of the Soghan region emphasising the Seghin complex fabric (modified from Angiboust et al., 2016). The lower hemisphere equal area stereographic projection depicts main foliation and studied fault attitudes. C. Pressure-Temperature (P-T) diagram showing the path followed by the upper blueschist-facies blocks from the Seghin complex together with Raman spectroscopy of carbonaceous material (RSCM) temperatures (after Angiboust et al., 2016). Peak conditions for the adjacent Ashin complex as well as inferred subduction thermal gradients are shown for comparison. For further details regarding phase stabilities and facies subdivision the reader is referred to Evans (1990) and Angiboust et al. (2016). MS—metasediment; Ser—serpentine; BS—blueschist; A—amphibolite-facies; BS—blueschist-facies; EBS—epidote blueschist-facies; EA—epidote amphibolite-facies; Ecl—eclogite-facies; GS—greenschist-facies; PA—pumpellyite actinolite-facies. Mineral abbreviations used along this paper are: Ab—albite; Act—actinolite; Amp—amphibole; Cal—calcite; Cb—carbonate; Chl—chlorite; Chm—chamosite; Clc—clinochlore; Cpx—clinopyroxene; Ep—epidote; Fac—ferro-actinolite; Gln—glaucofane; Jd—jadeite; Lws—lawsonite; Or—orthoclase; Pmp—pumpellyite; Ph—phengite; Py—pyrite; Qz—quartz; Ttn—titanite.

grain-fragment rotation as evidenced by the mismatch between foliated fragments and their respective counterparts (e.g., Fig. 2E). The slip boundaries between pristine and brecciated blueschists are sharp and subplanar (e.g., Fig. 2C and S1C), while brecciation intensity increases towards a discontinuously exposed fault core. At the meso-scale, shearing-related brecciation appears to be post-dated by further ductile shearing as evidenced by the development of a foliation within the matrix surrounding fragments. Extensional veins containing albite, glaucophane, lawsonite, phengite and pumpellyite crosscut pristine non-brecciated blueschist domains (e.g., Fig. S1C). Remnants from the same vein set are also found as breccia clasts within adjacent brecciated domains (Fig. 2E and S1C). Unlike higher grade prograde blueschist-facies veins showing shearing-related deformation parallel to the main foliation (Muñoz-Montecinos et al., 2021), the veins reported in this study developed as purely extensional structures devoid of viscous features.

Cohesive, ultrafine-grained zones with a darkish satin appearance (hereafter referred to as ultracataclastic veins) are associated with brecciated blueschists within the central region of the fault zone. These veins, that resemble pseudotachylytes (e.g., Lin, 2007), crosscut the host blueschist (Fig. 2F) and more commonly the breccias as thin injection (<5 mm-wide) or fault veins (<3 cm-wide), the latter with planar slip boundaries (Fig. 2F, 3A, B and C). Several layers of fault-related material commonly exhibit flow textures and streaks (Fig. 3B and C). Note that reworked ultracataclastic veins are observed as fragments in the brecciated domains (Fig. 3A).

**4. Microstructures and mineral chemistry**

Petrographic observations and petro-geochemical analyses, including thermodynamic modelling, on ultracataclastic veins, brecciated blueschists and extensional vein material have been per-

formed using (i) scanning electron microscope in back-scattered (SEM-BSE) and energy dispersive X-ray spectroscopy (EDS; including X-ray maps and estimates of the chemical composition of large scanned surfaces) modes, (ii) electron probe microanalyzer (EPMA; including defocused beam surface estimates), (iii) powder X-Ray diffractometry (XRD), (iv) in situ laser ablation-inductively coupled plasma-mass spectrometer (LA-ICP-MS) and (v) Perple\_X software (version 6.8.9). Details of the analytical techniques, parameters and software used are outlined in the supplementary material.

Micro-scale observations show that the fault breccia is composed of blueschist clasts and extensional vein fragments (Fig. 4A) enclosed in a very fine-grained foliated comminuted matrix (mostly <30 μm in diameter; Fig. S2A and S2B). The blueschist clast morphologies are subangular, containing mainly glaucophane (locally exhibiting actinolitic cores and/or rims) and pumpellyite (>50 vol.%) and minor lawsonite, phengite, chlorite, winchite, titanite and albite. The same mineralogy is present in the pristine foliated host blueschists and in the comminuted matrix, but chlorite and winchite are absent in the latter (Fig. 4B). In addition, Si-rich phengite (up to 3.7 a.p.f.u.; Fig. 5A), glaucophane and albite fringes occur in the interclast breccia matrix (Fig. 4A). Such features are not observed in the blueschist host, which is mostly devoid of phengite and albite, indicating that the phase-assemblage distributions cannot be envisioned by clast comminution alone, but involved the formation of new minerals. Note that structurally similar foliated cataclasites and blueschist breccias have been observed upstream in other high grade blocks, that contain abundant lawsonite and clinopyroxene and only very minor pumpellyite. In the studied locality, carbonate- and silicate-rich lawsonite-bearing vein fragments and vugs occur, the latter characterized by highly rounded and irregular morphologies apparently devoid of cataclastic imprint,



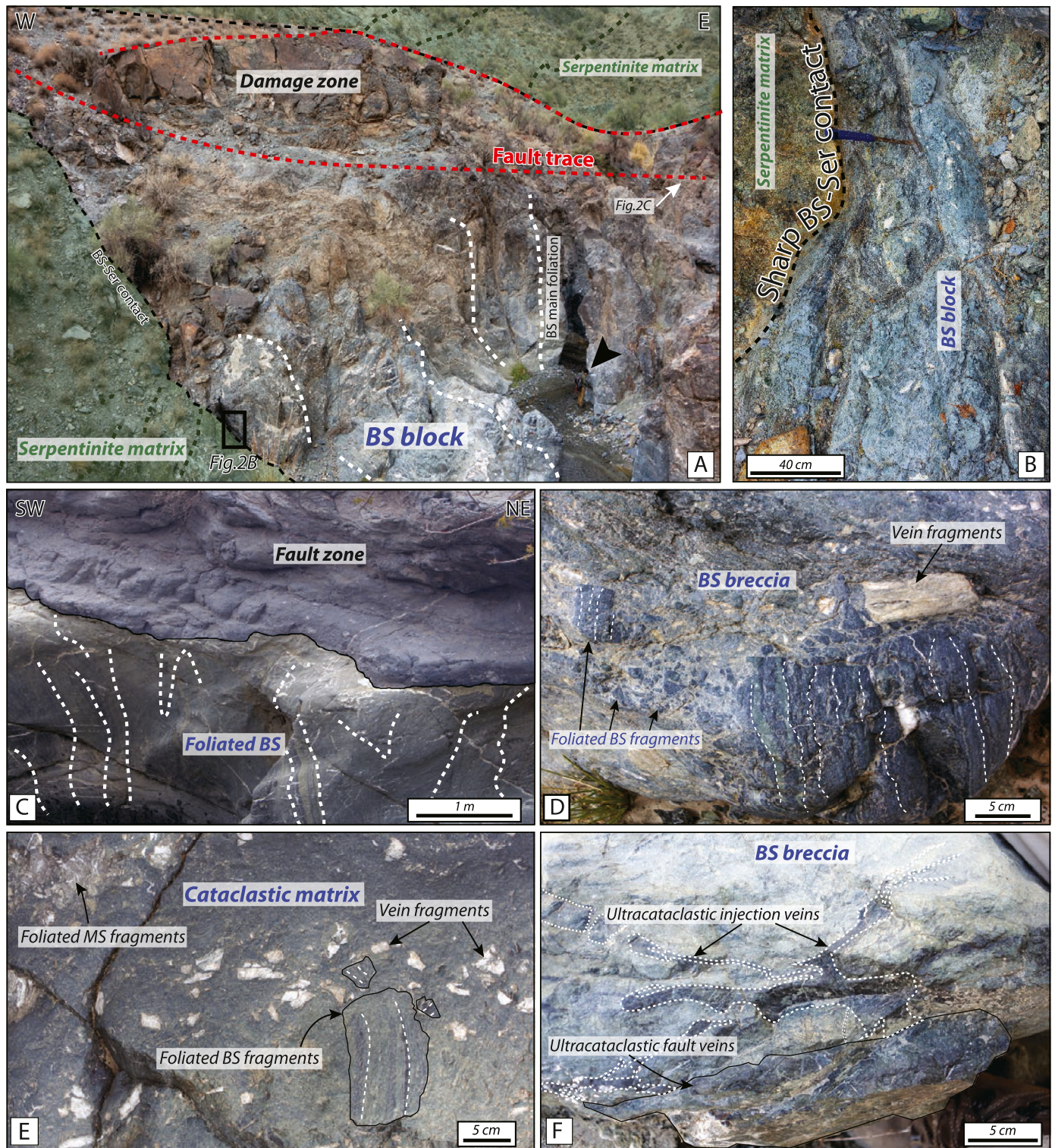


**Fig. 2.** Field pictures of the investigated fault zone from the Seghin complex. A. General view of the studied blueschist block surrounded by serpentine matrix. Note the fault features in the upper part of the image and the width ( $\leq 4$  m) of the well-preserved fault zone. Black arrow pointing to a geologist for scale. B. Detailed view of the sharp blueschist block-serpentine matrix contact. C. Crosscutting relationships between the fault zone and the pristine foliated blueschist block. Note how the fault crosscuts at high angle the main blueschist foliation. D. Blueschist breccia. E. Blueschist chaotic breccia showing highly angular and foliated blueschist, albite-glaucophane-phengite-bearing vein and metasedimentary fragments. F. Ultracataclastic injection and fault vein structures in a blueschist breccia. BS—blueschist; MS—metasediments.

likely representing crystallized fluid-filled cavities present during comminution (Fig. 4C). Glaucophane-lawsonite-phengite-bearing albite-rich vein clasts, identical in mineralogy to the aforementioned extensional veins, also occur in the fault breccias beside blueschist clasts. The contact between the brecciated blueschist

domains and the ultracataclastic veins is sharp and clean (Fig. 3D and 4A).

The ultracataclastic veins consist of several layers of dark-shaded regions (hereafter referred to as Brown and Black regions, respectively; see Fig. 3D) separated by sharp, subplanar slip bound-



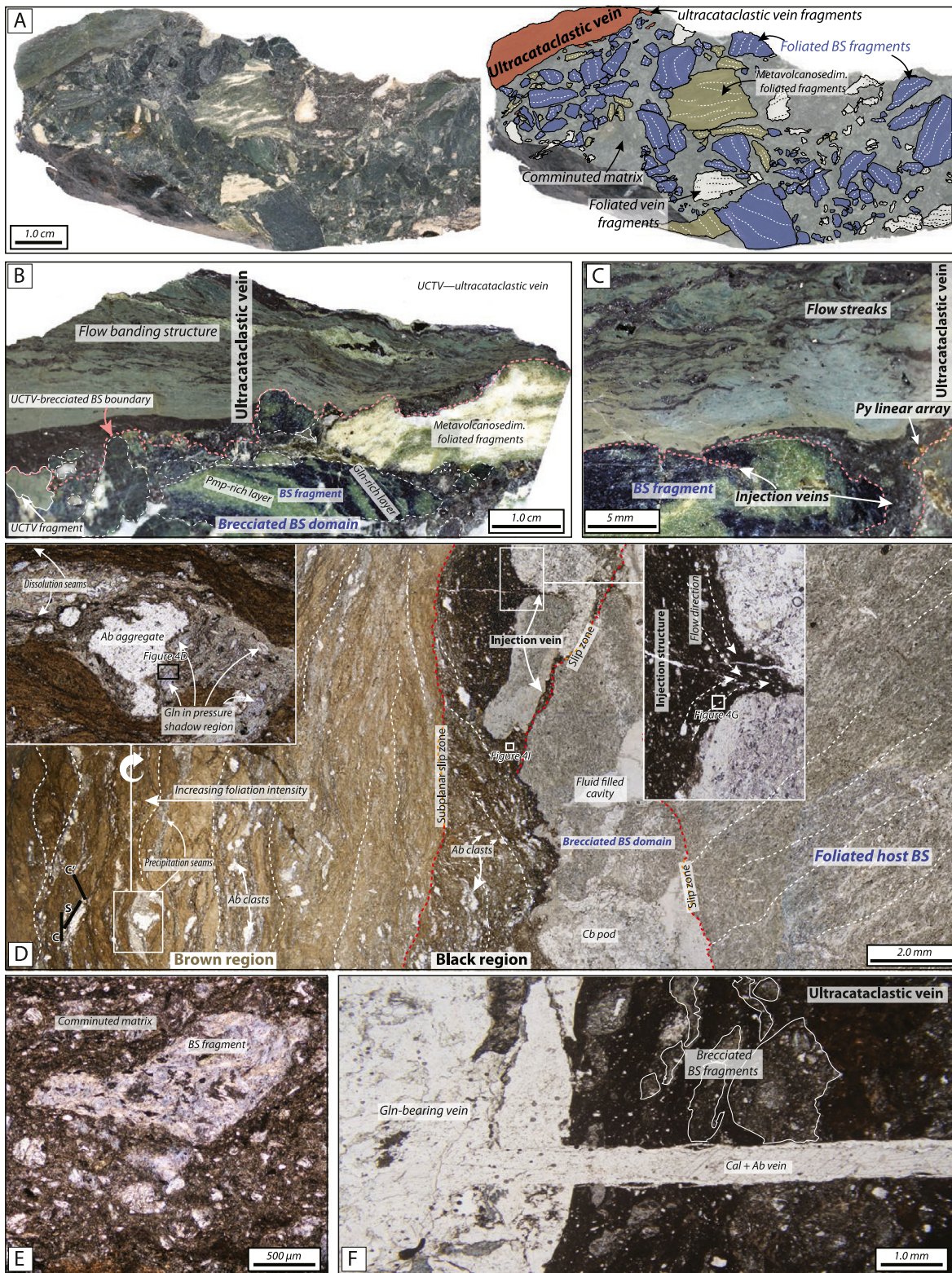


**Fig. 3.** Polished rock slab pictures (A to C) and thin section views (D to F) of representative samples from the Seghin complex fault zone. A. Complex brecciated blueschist showing a variety of fragments and a crosscutting ultracataclastic vein; reworked fragments of the ultracataclastic vein are also present as clasts in the breccia. The right-hand panel is a schematic representation emphasising relevant features. Note that millimetres-wide ultracataclastic vein fragments have been reworked and incorporated in the brecciated region. B. Picture highlighting the ultracataclastic vein-breccia contact and related surrounding features. C. Detailed picture of the ultracataclastic injection vein fabrics. Flow streaks of fault gouge materials as well as linear arrays of sulphides are visible. D. photomicrograph showing representative structural features of a brecciated blueschist and an ultracataclastic vein. Note the presence of (i) different layers of fault gouge material, (ii) mylonitic deformation, including S-C-C' fabrics, within the Brown regions, (iii) black dissolution and pale green precipitation seams, (iv) sharp slip boundaries between fault gouge material and against the brecciated domain, (v) injection and flow textures, (vi) albite-glaucophane-phengite ( $\pm$  lawsonite)-bearing vein fragments, (vii) sharp slip surfaces between brecciated and pristine blueschist and (viii) a pristine foliated blueschist host. E. Blueschist fragments incorporated into an ultracataclastic vein. F. Albite-glaucophane-phengite-bearing extensional vein crosscutting an ultracataclastic vein. Metavolcanosedim.—metavolcanosedimentary; UCTV—ultracataclastic vein. (For interpretation of the colours in the figure, the reader is referred to the web version of this article.)



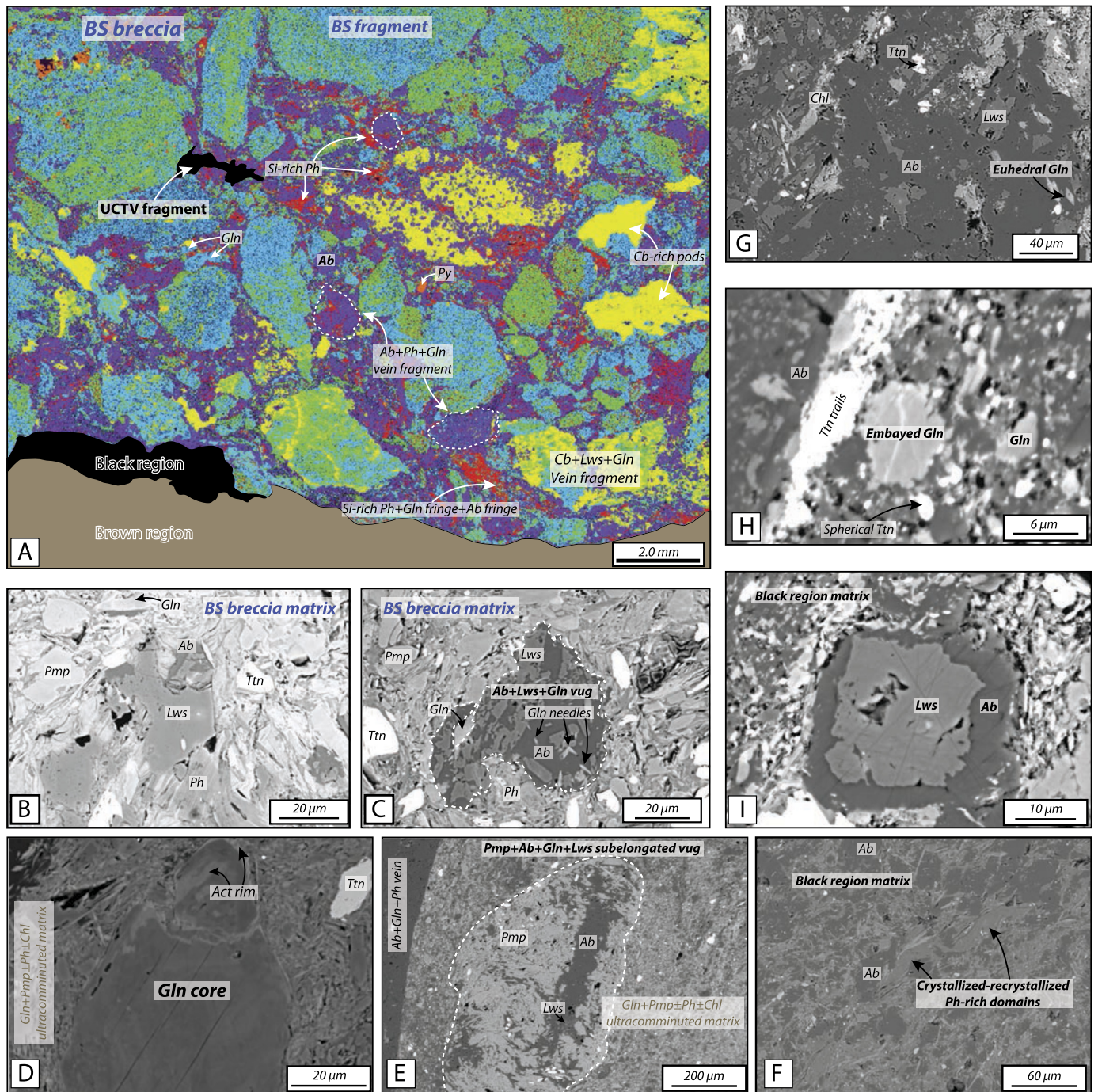


**Fig. 4.** A. Map image of selected phases from a blueschist breccia based on energy-dispersive X-ray (EDS) spectroscopy. The bottom part of the image has been masked out since the grain size is extremely fine and mineral identification is not possible at the ultracomminuted scale of the ultracataclastic veins. Note the presence of (i) a variety of clasts characterized by subrounded and subspherical morphologies, (ii) fringes filled by albite and Si-rich phengite, (iii) vein fragments (delineated by dashed white lines) and (iv) vugs that lack cataclastic imprints. Electron backscattered images (B to I). B. Image showing the ultracomminuted interclast matrix in the blueschist breccia. Note the highly angular crystal morphology. C. Subrounded vug filled by albite, lawsonite and glaucophane needles surrounded by ultracomminuted material. D. Pressure shadow domain from the Brown region around an albite aggregate as depicted in Fig. 3D. E. Elongated and rounded pumpellyite, albite and lawsonite vug in the Brown region. Note that pumpellyite crystals are elongated perpendicular to the margins (towards the centre of the vug; syntaxial growth) while albite and lawsonite are almost exclusively occurring in the vug centre. F. Black region microdomain composed mainly of newly formed or recrystallized albite and phengite. G. Black region microdomain composed of newly formed or recrystallized albite, glaucophane, pumpellyite, lawsonite and chlorite. H. Embayed and ultracomminuted glaucophane grains and titanite trails immersed in an albite matrix from the Black region. I. Replacement texture of a lawsonite grain rimmed by albite in the ultracomminuted Black region. (For interpretation of the colours in the figure, the reader is referred to the web version of this article.)

aries (Fig. 3B and D). Flow textures and streaks of alternating Black and Brown ultracataclastic vein materials are distinguishable and oriented subparallel to the slip surfaces crosscutting the brecciated blueschist domains. In general, the Black regions are located in the host-vein margins whereas the Brown layers are concen-

trated in the central part of the veins (Fig. 3B and D), the latter being commonly intruded by the former. The Brown regions are dominated by micrometre to submicrometre-sized pumpellyite and glaucophane, the latter partly replaced by actinolite and associated with minor albite, chlorite and phengite. Pumpellyite, glaucophane



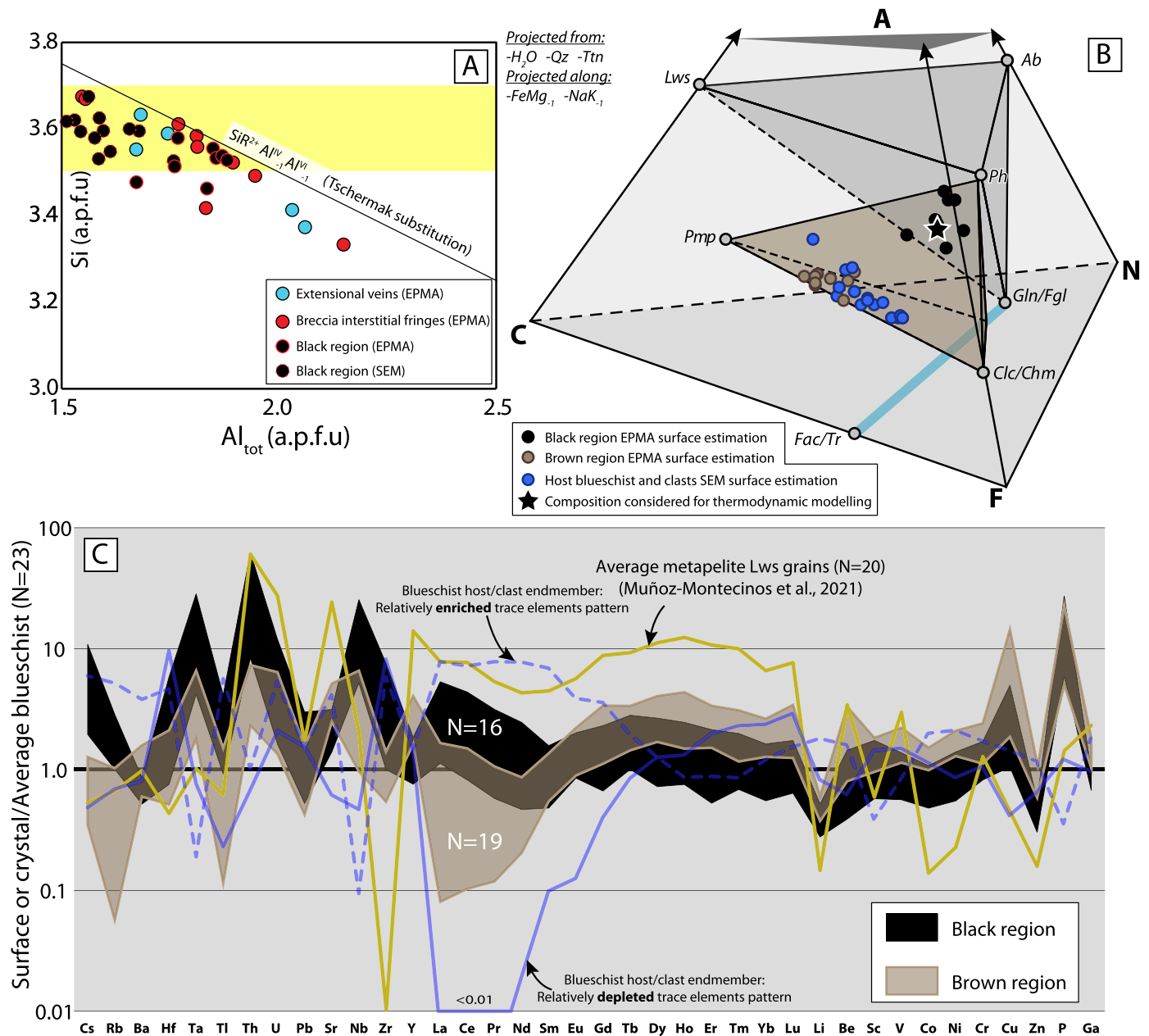


**Fig. 5.** A.  $Al_{tot}$  (a.p.f.u.) vs. Si (a.p.f.u.) in phengite from the Black regions, extensional albite-rich veins and breccia interclast fringes. SEM analyses with the best stoichiometric formula were selected. B. ACFN tetrahedral diagram projected from the phases and exchange vectors indicated. The chemical compositions used in this study were estimated by EPMA and SEM surface analysis (see methods section for details). This methodology is notably advantageous in highly heterogeneous rocks. Note that neither albite nor lawsonite are considered in the Brown region assemblage since these phases are derived from comminution or represent isolated vugs domains, respectively. C. In situ LA-ICP-MS trace element composition diagram of Black and Brown regions from ultracataclastic veins normalized to average pristine blueschists/clasts. The latter is obtained after averaging the results from the studied samples: SO1877 and SO1877.1. In addition, an average of 20 analysed metapelite-hosted lawsonite crystals from Muñoz-Montecinos et al. (2021) are shown for comparison and assumed to represent a metasedimentary signature since they are the main carriers of REEs, Th, U and Sr in such rocks. The bold and dashed blue patterns represent highly enriched and depleted blueschists host and clast endmembers. The number of analyses for each domain is 23, 16 and 19 for the blueschists, Black and Brown regions, respectively. (For interpretation of the colours in the figure, the reader is referred to the web version of this article.)

and minor chlorite and phengite are found as newly formed grains that overgrow the ultracomminuted matrix and cement interstices between larger fragmented grains. Irregular albite aggregates and clasts from former vein material are often associated with strain caps and shadows, the latter containing anhedral to euhedral fine to very fine-grained glaucophane and pumpellyite (Fig. 3D and 4D). In addition, some mineral fragments can also be present in the pressure shadow regions. These viscous patterns are better developed towards the internal region of the ultracataclastic veins where S-C-C' fabrics are present (e.g., Fig. 3D). Rare rounded and sub-elongated vugs containing pumpellyite, albite, glaucophane

and lawsonite are observed (Fig. 4E). Such domains may also represent minerals precipitated in fluid-filled pockets from former free fluids present during cataclasis. Note that lawsonite in the Brown region matrix has not been detected using X-ray diffraction techniques (Fig. S3C), although it has been rarely observed in vugs.

In Black regions (Fig. 3D), millimetres-wide injection structures occur infiltrating the brecciated blueschist domains and developing flow structures composed of (i) submicrometre, irresolvable material, (ii) ultracomminuted or embayed glaucophane, lawsonite, albite, phengite, pumpellyite and titanite fragments (Fig. 4H, S2D and E), (iii) millimetres-wide albite-rich vein clasts similar to those

observed in the host blueschist breccias, (iv) millimetres- to micrometres-wide albite crystals or aggregates in the matrix, commonly associated with newly formed, post-comminution anhedral to euhedral glaucophane, lawsonite and Si-rich phengite (3.5 to 3.7 a.p.f.u.; Fig. 4F, G, 5A and S2C) and (v) lawsonite overgrowths along fractured albite grains and/or albite cleavages as well as replacement of lawsonite by albite (Fig. 4G and I). These mineral occurrences were confirmed by X-ray diffraction analysis as shown in Fig. S3B. We note that newly formed glaucophane shows retrograde features such as actinolite rims and pumpellyite needles (Fig. S2D). These faulting-related textures (including the breccia matrix) have been affected by subsequent viscous deformation and development of a foliation (e.g., Fig. 3D, S2A and S2B). Millimetres-wide blueschist breccia and pristine blueschist fragments can be seen incorporated in the ultracataclastic veins (Fig. 3E and F). The brecciated domains of the damage zone are in sharp and subplanar contact with the pristine well-foliated blueschists as well as with the ultracataclastic veins (Fig. 3D). Last, some post-faulting extensional glaucophane- and (Si-rich) phengite-bearing, albite-rich veins crosscut all the forementioned fault-related features (Fig. 3F).

## 5. Geochemistry

Composition-space analysis of SEM and EPMA surface chemical estimates show that Brown regions compositions are comparable to those of pristine blueschist samples and breccia fragments (Fig. 5B). The ACFN projection indicates that Brown region bulk compositions can well be explained by an assemblage dominated by pumpellyite and Na-amphibole with minor phengite and chlorite (brown tie-tetrahedron in Fig. 5B). On the other hand, the composition of the Black regions is clearly displaced towards albite, reflecting enrichments in  $\text{Al}_2\text{O}_3$  and  $\text{Na}_2\text{O}$  components, and can be explained by the lawsonite-glaucophane-albite-phengite mineral assemblage (grey tie-tetrahedron in Fig. 5B), in agreement with the observed parageneses.

Rasterized LA-ICP-MS results on the different studied domains are shown in the spider diagram from Fig. 5C, normalized to the averaged pristine blueschists and host fragments (hereafter referred to as average blueschist). The Brown regions trace element patterns are characterized by negative anomalies in Rb, Tl and in most Light Rare Earth Elements (LREEs), whereas elements such as Ta, Th, Sr, Nb, Y, Cu, P and Heavy Rare Earth Elements (HREEs) are enriched relative to the host pristine and brecciated blueschists. Unexpectedly, somewhat different trends are observed in the trace element patterns from the Black regions. The most important anomalies correspond to markedly higher contents of Cs, Rb, Ta, Th, U, Nb, Cu and P relative to the average blueschist.

## 6. Discussion

### 6.1. P-T conditions of faulting

Field and petrological characterization (this study), together with previous thermometric results (Agard et al., 2006; Angiboust et al., 2016), indicate that the Seghin complex formed by the gathering of lenses with resolvable P-T differences ( $\sim 150^\circ\text{C}$  and several kilobars) in a serpentinite channel. The fault zone and the host blueschist investigated here reveal the occurrence of lawsonite blueschist-facies mineral associations characterized by glaucophane, pumpellyite, lawsonite, Si-rich phengite and albite.

P-T conditions of faulting are evaluated through thermodynamic modelling in two domains corresponding to the Black and Brown regions. This approach is assumed to be valid in the host blueschist since the pumpellyite and glaucophane-rich domain compositions are virtually identical to that of the Brown regions

(e.g., Fig. 5B). The chemical compositions were acquired after averaging defocused beam surface estimates in the system  $\text{Na}_2\text{O}-\text{CaO}-\text{K}_2\text{O}-\text{FeO}-\text{MgO}-\text{Al}_2\text{O}_3-\text{SiO}_2-\text{H}_2\text{O}-\text{O}_2$  (Table S2). Both pseudosections were computed in the range 200 to 500 °C and 0.2 to 1.5 GPa under water-saturated conditions. Selected solid solution models are summarized in Table S3. For the following pseudosection analysis, we only consider observed and measured mineral assemblages and their mineralogical and chemical composition of newly formed/recrystallized domains. The purpose of this approach is to roughly constrain ambient P-T conditions of faulting rather than potential – although unlikely – flash heating temperatures reached during fast slip. In the Black regions, natural mineral occurrences and abundances are in relatively good agreement with the calculated field predicting major amounts of albite and Na-amphibole together with moderate lawsonite, phengite ( $\sim 70$  vol.%; see Fig. 6 for details), clinopyroxene and minor quartz. Glaucophane composition predicted in the pseudosection is analogue to measured compositions of Na-amphibole (Table S1). Calculated Si-in-phengite isopleths intersect the best-fit field as shown in Fig. 6, in agreement with measured crystals (see Fig. 5A and Table S1). In addition, the occurrence of lawsonite and albite and the lack of peak pumpellyite and actinolite in the Black regions, allow us to infer faulting conditions in the range of 0.6–1.0 GPa and 230–300 °C (lower blueschist-facies). A retrograde stage associated with final exhumation is characterized by the occurrence of thin actinolite rims around glaucophane and pumpellyite aggregates ( $\pm$ albite) which likely took place below the Na-Amp-in curve, in the pumpellyite stability field (Fig. 6). A similar approach applied in the Brown regions domain yields similar faulting metamorphic conditions in the range 0.6–1.0 GPa and 280–300 °C (Fig. S3A).

This approach is subject to uncertainties inherent to the former ultracataclastic processes, namely, the mixing of material that is originally not in thermodynamic equilibrium. Nevertheless, as stated previously, our calculations consider micro-domains in which apparently newly formed (or recrystallized) grains occur implying – at least – local equilibrium. In addition, our thermodynamic calculations predict the occurrence of peak clinopyroxene and minor quartz which were not observed in the natural samples. This discrepancy may derive from slight imprecision in effective bulk composition, but other factors such as uncertainties in the solution models, fluid composition and/or oxygen fugacity may also have an effect. In the host blueschist, the occurrence of minor amounts of lawsonite may indicate slightly higher peak pressure conditions or little imprecision in the modelled bulk composition. Overall, the relatively good agreement between observed and predicted mineral paragenesis (e.g., Evans, 1990) confirms the relative robustness of the inferred P-T conditions for the fault rocks.

In addition to pseudosection modelling, inferred HP-LT conditions of faulting are supported by (i) the presence of Si-rich phengite and glaucophane as fringes and lawsonite-bearing vugs in the matrix of blueschist breccias (interpreted as minerals precipitated from HP fluids in fault zone porosity), (ii) the growth of newly formed, euhedral glaucophane and lawsonite in ultracataclastic vein fluid-filled vugs and (iii) mutually crosscutting-reworking relationships between faulting-related ultracataclastic veins and glaucophane-phengite-bearing extensional veins. The resulting P-T conditions are interpreted as the crystallization and/or recrystallization of the fluidized fault gouge material right after seismic sliding (see below) in the lower blueschist-facies. Such features were progressively obliterated by ongoing viscous shearing (e.g., Lin, 2007) as evidenced by the occurrence of solution seams and pressure shadows filled by glaucophane and pumpellyite, indicating HP-LT conditions during dissolution-precipitation processes. Thus, brittle faulting, extensional hydrofracturing and viscous creep all coevally occurred in the depth range 20–35 km, as illustrated in Fig. 7 and 8.



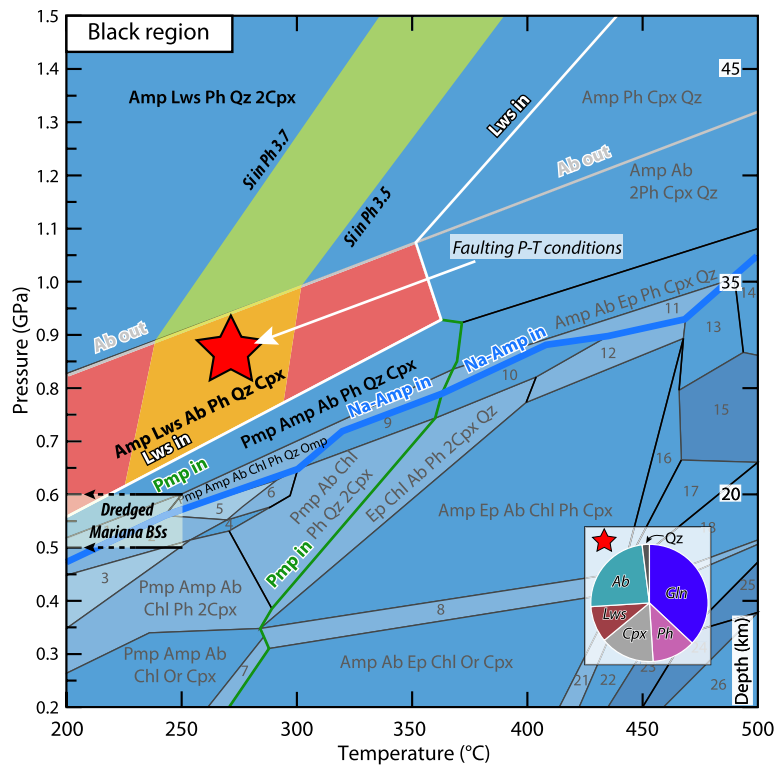


**Fig. 6.** Pseudosection for the Black regions composition. The red fields highlight the best-fitting mineral assemblages and abundances. The yellow area corresponds to Si-in-phengite isopleths of 3.5 to 3.7 (see Fig. 5A). Pie-chart shows mineral modes (in vol.%) at the P-T conditions indicated by the red star. However, the actual faulting conditions are depicted by the intersection between Si in phengite isopleths and the red field. Dredged Mariana blueschist field represents inferred P-T conditions from Maekawa et al. (1993). Relevant reaction curves are marked as thick coloured lines. Parageneses in the fields marked with numbers are detailed in a table in Fig. S3.

### 6.2. Deciphering deformation and fluid circulation processes

Close spatial associations between ultracataclastic veins and brecciated blueschists (Fig. 2B) and the occurrence of reworked ultracataclastic vein fragments in breccias, witness for an episodic nature of faulting resulting in the formation of a large palette of rock fabrics and structures. The intrusive character of ultracataclastic veins, as well as the occurrence of flow and injection fabrics are features known in pseudotachylytes and fluidized ultracataclasticites reported in other paleo-subduction environments (e.g., Rowe et al., 2005; Meneghini et al., 2010). Whichever the case, fast, seismically-generated events seem the best candidates to account for such structures (Rice, 2006; Ujiie et al., 2007; Lin, 2011; Rowe and Griffith, 2015). Although X-ray diffraction patterns and microscopic observations show that ultracomminuted crystalline material is the main constituent of the ultracataclastic veins, the shape of their diffraction base lines at low angles (Fig. S3B and S3C) together with the presence of (i) embayed grains, (ii) pyrite and Ti-oxides trails and (iii) elongated and rounded fluid-filled vugs similar to amygdules (Fig. 3C, 4E, 4G, 4H and S2E), may indicate that some melt could have formed during frictional sliding (Magloughlin and Spray, 1992; Rowe et al., 2005; Lin, 2007; Meneghini et al., 2010). Recently, similar features have been observed in shallower environments and interpreted as former melt products (pseudotachylytes; see Ujiie et al., 2021). However, we cannot unequivocally establish that a frictional melt has been once present in the studied fault zone.

The ultracomminuted material appears to have behaved as a fluidized fluid-solid system capable of forming complex flow and injection structures (e.g., Ujiie et al., 2007). Lin (2011) reported strikingly similar structures and inferred that fluidized ultracataclasticite formation resulted from a recent (2008) Mw 7.9 earthquake, emphasising coseismic shearing as a mechanism capable of flu-

idization and injection of fine-grained material virtually devoid of frictional melts. Mutual crosscutting relationships among several ultracataclastic domains indicate synchronous formation during similar seismic events (e.g., Rowe et al., 2005; Lin, 2011).

Sharp slip surfaces, including injection structures approaching the brecciated blueschist host (e.g., Fig. 3A to D), demonstrate that fault propagation generally proceeds towards the host breccia and blueschist domains rather than via fast re-shearing of the previously-generated ultracataclasticite (e.g., Collettini et al., 2009). This statement is supported by contrasted major and trace element signatures among Black and Brown regions indicating different sources (Fig. 5B and C). It is thus inferred that brecciated blueschist domains are mechanically weaker than fault core lithologies, provided that fault gouge interstices become cemented at short timescales (e.g., Kay et al., 2006; e.g., Fig. 3D and 4D). This possibility is supported by experimental investigations showing that incremental slip in a fault zone results in progressive fault gouge strengthening (Ujiie et al., 2009). These observations demonstrate that fluid-assisted cementation of the ultracomminuted matrix could potentially have occurred during interseismic periods associated with viscous creep (e.g., Lin, 2007; Di Toro et al., 2009). In addition, crosscutting relationships of pristine extensional or fragmented veins filled by HP-LT mineral assemblages, as well as the presence of similar mineral paragenesis filling vugs and fringes along the brecciated matrix, demonstrate that hydrofracturing and high pore fluid pressure conditions were also cyclically attained and temporally compatible with a sequence of seismic faulting events.

The composition of the Brown regions is similar to pristine blueschists and blueschist fragments, while the Black regions are substantially shifted towards the albite endmember (Fig. 5B). These contrasted compositions indicate that the Brown regions were produced by ultracomminution of the host blueschist and breccia

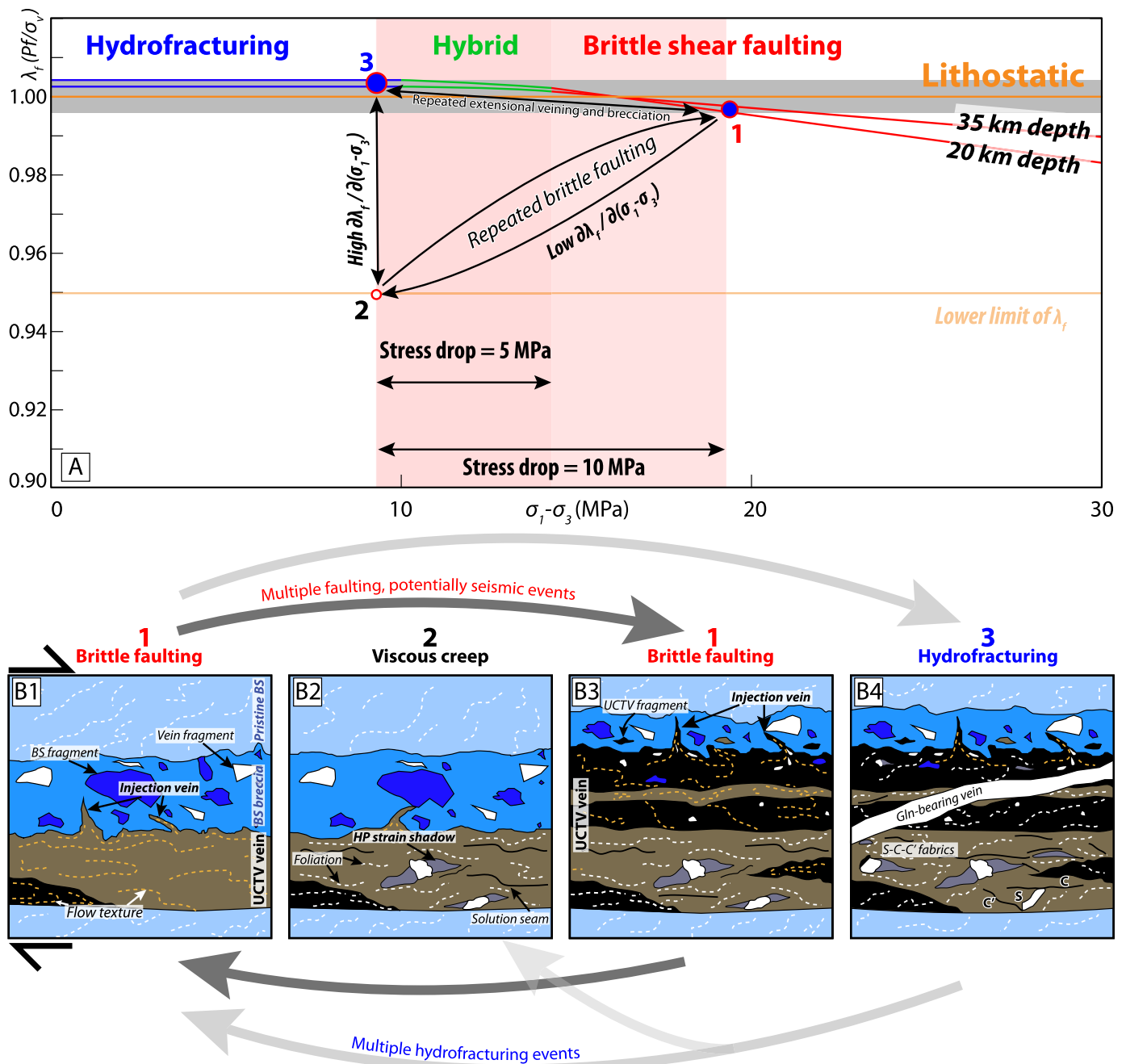


**Fig. 7.** Structural and mechanical evolution sketches of fault rock fabrics from the Seghin complex. A.  $\lambda_f$  vs.  $\sigma_1 - \sigma_3$  diagram for the compressional regime state calculated for 20 and 35 km depths, corresponding to inferred faulting P-T conditions. An Andersonian stress state is assumed where for a compressional setting  $\sigma_v = \sigma_3$ , whereas for an extensional regime  $\sigma_v = \sigma_1$ . For the sake of simplicity, only the compressional regime is shown (see discussion section for details). The failure envelopes were constructed following the mathematical formulation detailed in Cox (2010). The parameters used are density=3000 g/cm<sup>3</sup>; gravity acceleration=9.8 m/s<sup>2</sup>; friction coefficient=0.45; tensile strength of a blueschist (basaltic) rock mass=2.5 MPa; Cohesion=5.2 MPa. The lower limit of  $\lambda_f$  corresponds to the minimum value calculated in Angiboust et al. (2015) and is based on exhumed subduction-related petrofabrics inferred to have formed at blueschist-facies depths. Justification and references regarding parameter selection are given in the Supplementary Material. B1 to B4. Fabric evolution sketches associated with  $\lambda_f$  vs.  $\sigma_1 - \sigma_3$  variations. The thick bold black and grey arrows aim at representing cyclicity in the different events. Note that after any hydrofracturing event at point 3 (e.g., panel B4) the  $\lambda_f$  vs.  $\sigma_1 - \sigma_3$  path may potentially evolve directly towards point 1 or 2 (or any intermediate state between point 2 and 3) before subsequent stress recovery and reaching point 1 once again (or another hydrofracturing event). (For interpretation of the colours in the figure, the reader is referred to the web version of this article.)

while Black regions incorporated considerable amounts of albite vein component. Textural evidence demonstrating that albite clasts are more abundant in the Black regions also reflects this discrepancy (e.g., Lin, 2007). Nevertheless, trace element analyses show marked anomalies among the different ultracataclastic vein domains relative to the average blueschist standard pointing to sim-

ilar metasomatic processes affecting both domains. Thus, the observed shift cannot be explained solely by mechanical mixing and homogenization of fault zone material (Fig. 5C).

Strong Cs and Rb negative anomalies in the Brown regions while the same elements are abundant in the Black regions reflect relative depletions and enrichments in phengite, the main Large-



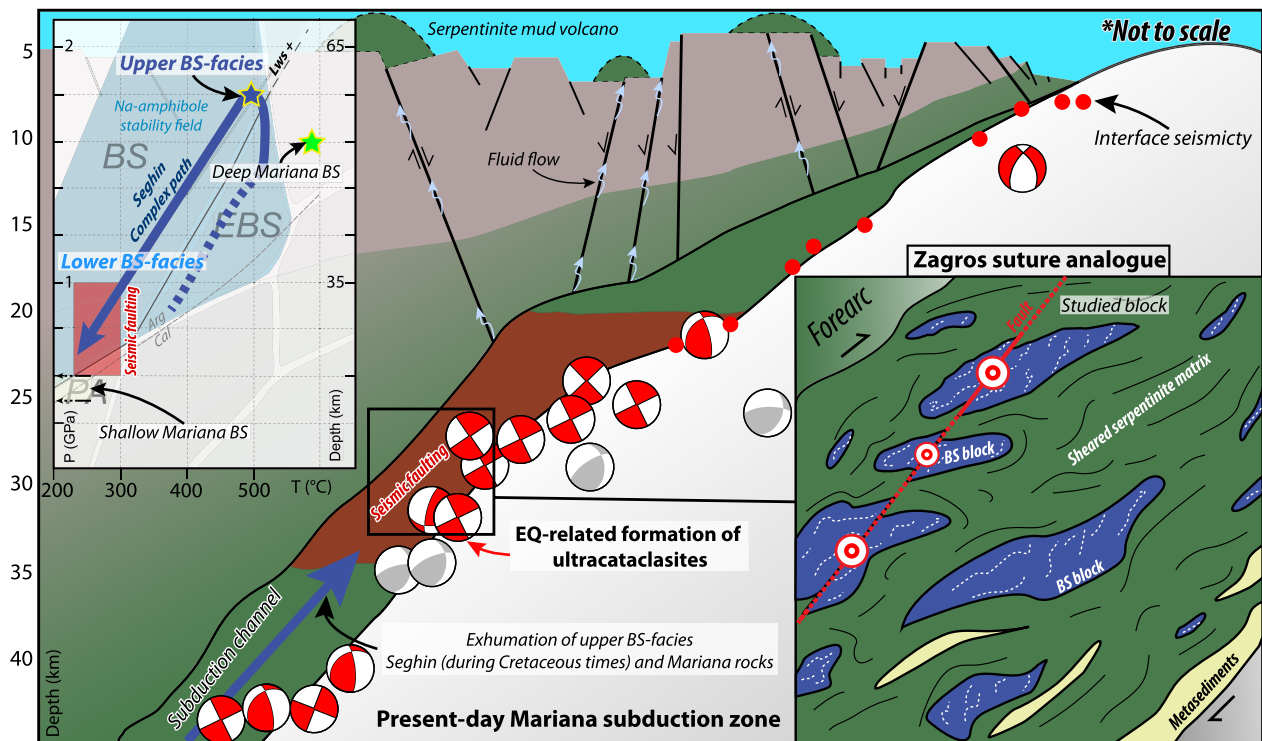


**Fig. 8.** Subduction sketch (modified from Fryer et al., 2020) and relocated focal mechanisms (red for thrusting and grey for extension; within errors) from 2003–2004 moderate magnitude earthquakes (Emry et al., 2011). The red dots represent well-resolved earthquake locations inferred as representing the subduction interface (after Oakley et al., 2008). The inset is a schematic representation of how the subduction channel (not to scale) would look like using the Seghin complex as an exhumed analogue. Note the fault trace cutting across blocks and the serpentinite matrix. Dark blue colour represents higher grade blueschist blocks (e.g., Angiboust et al., 2016; Muñoz-Montecinos et al., 2021). The red region in the subduction channel depicts calculated faulting depths for the Seghin complex, while the lower blueschist field corresponds to conditions inferred for recent blueschist-facies metamorphism by Maekawa et al. (1993). The P-T inset compiles relevant metamorphic (Maekawa et al., 1993; Angiboust et al., 2016; Tamblyn et al., 2019) and faulting conditions (this study). EQ—earthquake. (For interpretation of the colours in the figure, the reader is referred to the web version of this article.)

Ion Lithophile Elements carrier in the system (Fig. 5C). In both domains, substantial Nb and Ta positive anomalies are observed relative to the host breccias and pristine blueschists. Th and HREEs enrichments are also observed in the Brown and Black regions relative to the average and two blueschist compositions selected for comparison (Fig. 5C). These two compositions correspond to analyses containing the highest and the lowest amount of trace element abundances allowing to detect true enrichments (or depletions) that cannot be explained by ultracomminution of the host materials. Thus, strong Ta, Th, Nb and HREEs positive anomalies require an external source to match the values measured in the ultracataclastic vein domains. It is worth noticing that measured albite vein crystals show Ta, Th, Nb and REEs abundances commonly below 0.1 ppm and cannot be considered as the source of any anomaly.

Similar Ta and Nb (and Ti) anomalies have been reported in metasomatic eclogite lithologies from the Tianshan (China) and attributed to titanite dissolution during blueschist to eclogite-facies dehydration reactions and further long-distance transport before precipitation as veins (Gao et al., 2007). Considerable positive P anomalies are also observed in the Brown and Black regions likely reflecting exceptionally high amounts of apatite relative to the host blueschists. Similarly, Cu is also enriched only in the Brown and Black regions possibly associated with the presence of higher amounts of Cu-bearing phases such as chalcopyrite. In addition, strong Th and HREEs (and LREEs) positive anomalies are noticed in metapelite lawsonite crystals from the Seghin complex, the latter serving as a proxy of a metasedimentary-derived signature (Muñoz-Montecinos et al., 2021; see average metapelite lawsonite grains in Fig. 5C). Therefore, it is stated that the observed trace element anomalies (Ta, Th, Nb, HREEs, Cu and

P) represent a fingerprint of externally-derived mixed metamorphic fluid contributions associated with open-system behaviour during fluid circulation as reported in other subduction settings (Gao et al., 2007; Meneghini et al., 2010; Muñoz-Montecinos et al., 2020). Externally-derived fluid infiltration has been proposed by Muñoz-Montecinos et al. (2021). The authors concluded that metasedimentary and mafic/ultramafic-derived fluids were injected in the Seghin complex during prograde burial to near-peak conditions in the form of upwards traveling fluid pulses (e.g., Frank et al., 2015). These pulses were possibly associated with deep-seated metamorphic reactions taking place at greater depths than Seghin upper blueschists peak conditions (Muñoz-Montecinos et al., 2021). In contrast, the inferred fluid-rock interactions in the studied fault zone occurred at lower blueschist-facies conditions, once the Seghin complex was constituted as an uprising serpentinite mélangé emplaced at seismogenic depths at near 35 km depth. Thus, deeply-generated fluids may have travelled upwards along the subduction interface-channel and reached the seismogenic region where active fluid circulation through the different fault domains and seismic cycle stages occurred (e.g., Angiboust et al., 2014).

### 6.3. Modelling fluid - stress feedbacks in a blueschist-facies fault zone

To explain the episodic nature of the inferred brittle-viscous deformation events, a failure mode diagram considering pore fluid pressure vs. stress state variations has been constructed following the procedure detailed in Cox (2010; see caption from Fig. 7 for details). In this diagram, fluid pressure is represented by the pore fluid factor  $\lambda_f$  ( $P_f/\sigma_v$ ) and the stress state by the differential stress  $\sigma_1 - \sigma_3$  (in MPa), where  $P_f$  is the fluid pressure and  $\sigma_v$

the vertical stress. In order to compare our structural observations with modern subduction analogues, we assume a stress drop (difference of stress state after and before an earthquake) of 10 MPa, as inferred for mean thrust earthquakes from active subduction settings such as in Hikurangi and Mariana (Abercrombie et al., 2017; Bird, 1978). A lower stress drop of 5 MPa is also depicted for comparison. These values may represent upper boundaries since Coulomb wedge theory applied in active subduction margins requires a very weak megathrust to maintain force balance close to an equilibrium state, underscoring the role of overpressurized fluids (see below; e.g., Dielforder et al., 2020).

Our mechanical model reveals that the observed fabrics can be explained by stress and pore fluid pressure fluctuations (Fig. 7A). Assuming a brecciated blueschist as a starting point (i.e., after a hydrofracturing event), seismic faulting will potentially occur once  $\lambda_f$  vs.  $\sigma_1$ - $\sigma_3$  reach the brittle faulting failure envelope from Fig. 7A (point 1). At these conditions, pore fluid pressure must be high, near to lithostatic, to promote seismic faulting and explain the observed ultracataclastic injections crosscutting the host blueschists and breccias (Fig. 7B1). This brittle event is followed by poroelastic relaxation and fluid drainage, as a consequence of syn-faulting permeability increase, allowing  $\lambda_f$  and  $\sigma_1$ - $\sigma_3$  to drop until reaching point 2 (Fig. 7A; Cox, 2010, see also Sibson, 2013). During interseismic periods, fluid-present viscous deformation occurs as evidenced by the observed fabrics associated with pressure-solution processes, possibly strengthening the fault gouge previously generated (Fig. 7B2). Recovery of low  $\partial\lambda_f/\partial(\sigma_1-\sigma_3)$ , likely associated with sealing-induced permeability reduction and tectonic loading, allows for  $\lambda_f$  and  $\sigma_1$ - $\sigma_3$  build up until reaching the failure envelope at point 1 again. This triggers a new earthquake, as evidenced by the injection of newly formed ultracataclasites and brecciation in the margins of the faulting region (Fig. 7B3). Thus, seismic faulting-viscous creep cyclicity requires that fluid pressure must remain high, nearing the lithostatic threshold (e.g., Angiboust et al., 2015). This scenario is evidenced by the presence of fluidized fabrics as well as by the occurrence of vugs and fringes filled by HP-LT minerals interpreted as former fluid-filled cavities. Besides faulting activity, cyclic hydrofracturing is also testified by mutually crosscutting occurrences of extensional veins (e.g., Fig. 3F) and their brecciation (e.g., Fig. 2E, 3D, 4A and S1C). Note that this process is possible only if a high  $\partial\lambda_f/\partial(\sigma_1-\sigma_3)$  build-up occurs. To accomplish for these sudden pore fluid pressure highs, in situ dehydration of metabasaltic material or injection of external fluids are possible candidates. The former case is very unlikely since at these conditions, materials forming the Seghin complex were on their way upwards in the serpentinite subduction channel and water-consuming reactions are expected (Muñoz-Montecinos et al., 2021). We herein favour the latter case, where highly pressurized fluids originating from deep-seated dehydration reactions, infiltrate the Seghin complex sequence allowing for reaching again near-lithostatic  $\lambda_f$  (point 3 in Fig. 7A), promoting hydrofracturing, veining and subsequent pore fluid pressure drop (Fig. 7B4).

#### 6.4. A window onto Mariana-type subduction-related seismicity?

Investigations in dredged blueschist fragments from the Mariana subduction zone yield upper to lower blueschist-facies peak metamorphic conditions (Tamblyn et al., 2019 and Maekawa et al., 1993, respectively), comparable to those recorded by some of the peak blueschist blocks and the fault zone herein investigated, respectively. Thus, our findings demonstrate that the Seghin complex can be considered as a world-class, on-land analogue to the current seismogenic window of the Mariana margin (Maekawa et al., 2004; Fryer et al., 2020; Muñoz-Montecinos et al., 2021). In this tectonic configuration, active seismicity is characterized mostly by small- and moderate-magnitude earthquakes (e.g., Eimer et al.,

2020) whereas  $M_w > 7$  events are scarce (Emry et al., 2011). Focal mechanisms inferred from well-resolved moderate-magnitude earthquakes ( $M_w$  4.9-5.8), show that most seismic activity is associated with thrusting near the subduction interface-channel (Emry et al., 2011; Fig. 8). These and other lower magnitude events cluster at depths in the ranges 10 to 30 km and 45 to 60 km (Emry et al., 2011; Eimer et al., 2020), well within the calculated 20 to 35 km depths estimated for Seghin complex paleo-earthquakes.

A  $M_w \sim 5$  earthquake requires a rupture area in the order of  $10 \text{ km}^2$  and a total slip of few tens of centimetres (Sibson, 1989). The spatial dimensions of the Seghin complex, including the occurrence of several hectometre-sized blueschist blocks enclosed in a serpentinite matrix, are compatible with measured moderate-magnitude earthquake source properties. Using structural and kinematic observations, it was neither possible to state whether the studied fault system was reverse or normal nor whether faulting events also affected the serpentinite matrix around or other mafic blocks. Note, however, that our main conclusions regarding episodic faulting and fluid pressure cyclicity would remain mostly unchanged if the studied features were produced by normal faulting. Moreover, we suspect that the fault may have propagated through the serpentinite matrix around since localized deformation in the form of cataclastic fabrics were also observed therein and in other HP blocks (e.g., Muñoz-Montecinos et al., 2021; Fig. 8 and S1A). Experimental results on serpentinites and serpentinite gouge materials show that these fabrics may result from localized seismic slip interspersed with distributed stable creep (Reinen, 2000). In addition, it has been shown that transient changes on pore fluid pressures and/or slip velocities may trigger the mechanical transition from velocity-strengthening to velocity-weakening behaviour, thus promoting transient unstable slip (Moore et al., 1997; Reinen, 2000; Proctor et al., 2014). Lower magnitude earthquakes (e.g.,  $M_w \sim 4$ ) would also be associated with the rupture of single hectometre-sized blocks, also in line with Mariana-type seismicity.

The episodic nature of fluid pressure and stress build up is a compelling evidence for a seismogenic zone alternating between low and high  $\partial\lambda_f/\partial(\sigma_1-\sigma_3)$  regimes (Fig. 7). These variations are interpreted here as short-term seismicity recurrence (Emry et al., 2011) switching with longer-term, transient fluid circulation along the subduction channel as highly pressurized fluid pulses (Frank et al., 2015). Muñoz-Montecinos et al. (2021) suggest that fluid pressure build-up intensities are higher at greater depths, where massive hydrofracturing occurred in the mafic blocks near the eclogite-to-blueschist transition, vanishing at shallower conditions (see also Muñoz-Montecinos et al., 2020). These statements correlate well with high  $V_p/V_s$  ratios imaged in the Mariana setting in the depth range of 70 to 120 km (eclogite-facies depths), interpreted as slab dehydration processes (Barklage et al., 2015). Interestingly, high  $V_p/V_s$  conditions were also imaged in the depth window between 20 to 30 km (Barklage et al., 2015), suggesting that high pore fluid pressure conditions are also attained in the seismogenic region. On a rheological perspective, Wang et al. (2020) suggested that the scarcity of aftershocks in the shallow mantle wedge corner after the Maule megathrust earthquake ( $M_w$  8.8; Chile) is due to the velocity-strengthening behaviour of lizardite/chrysotile while the deeper occurrence of antigorite-rich patches allow for down-dip aftershock generation. Wang et al. (2020) emphasize that a similar rheological behaviour is expected in settings where buoyant serpentinite-rich subduction channels are able to flow updip, such as in Mariana-type margins. The proposition of Wang et al. (2020) supports the herein suggested scenario where earthquakes may have propagated through the foliated antigorite-rich matrix (see also Tarling et al., 2018).

In Mariana-type margins, two hypotheses are commonly invoked to explain the lack of large-scale earthquakes (see Emry et



al., 2011 and references therein for more details). In the first instance, it has been proposed that a weak serpentinized mantle – commonly thought to behave as a velocity-strengthening material – is capable of inhibiting earthquake nucleation (Hyndman et al., 1997). The other hypothesis invokes a weak coupling state of the plate interface due to very low normal stresses (e.g., Scholz and Campos, 2012). Our field-based investigation demonstrates that earthquakes may well occur within a highly serpentinized subduction channel in agreement with geophysical observations (e.g., Emry et al., 2011). In addition, our structural-mechanical inferences suggest that near to supra-lithostatic fluid pressure conditions (Fig. 7) are a prerequisite to maintain the system in a critically unstable mechanical regime, capable of promoting seismicity in the Mariana and other similar subduction margins such as the Izu-Bonin, Hikurangi, South Tonga and Kermadec (see for instance the  $M_w = 8.1$  earthquake that occurred at c. 20 km depth in the Kermadec subduction on March 4th, 2021; see also Scholz and Campos, 2012; Fig. 8). Therefore, we conclude that local fluid pressure highs promote seismic faulting in some patches (e.g., the studied blocks and their surroundings), while adjacent regions at lower fluid pressure conditions will potentially behave aseismically arresting earthquake nucleation and/or propagation (Scholz and Campos, 2012; Wang et al., 2020). Even though similar cataclastic fabrics are not reported so far (to our knowledge) in other similar localities (e.g., Franciscan complex), we speculate that such seismic-related features must have widely occurred but were in most cases overprinted due to exhumation-related metamorphism and deformation or, remain to be recognized in the geological record.

## 7. Conclusions

Our investigations demonstrate that the Seghin complex represents an extremely well-preserved fragment of a paleosubduction channel that likely evolved into a tectonic setting analogue to modern Mariana-type margins, where large-scale return flow enables the exhumation of HP-LT metamorphic rocks from depths of ~55 km up to the inferred seismogenic region near 25 km depth. We herein document the finding of a several meters-wide fault zone, comprising a variety of fabrics, including some produced by blueschist-facies paleo-earthquakes. Combining structural features with a mechanical modelling approach, we show that (i) stress accumulation must proceed faster than pore fluid pressure build-up in order to trigger moderate-magnitude seismicity and (ii) pore fluid pressure build-ups should be faster relative to stress build-up to explain the observed hydrofracturing pattern at seismogenic depths. In both cases, fluid pressure must be maintained at near-lithostatic values in order to explain the investigated rock fabrics, as indicated by high  $V_p/V_s$  ratios in the seismogenic region of the Mariana margin. Enrichments in Ta, Th, Nb, and HREEs indicate that external, possibly deep-seated fluids were capable of maintaining pore fluid pressures at critically high levels in order to trigger the inferred mechanical instabilities. Thus, the Seghin fault system provides an unprecedented opportunity to document the complex feedbacks between fluctuating pore fluid pressures and stress evolution in active Mariana-type subduction settings and help refining our understanding of earthquake-related processes in serpentinized subduction channels.

## CRedit authorship contribution statement

**Jesús Muñoz-Montecinos:** Conceptualization, Investigation, Methodology, Supervision, Validation, Visualization, Writing – original draft, Writing – review & editing. **Samuel Angiboust:** Conceptualization, Funding acquisition, Investigation, Methodology, Project administration, Supervision, Validation, Visualization, Writing –

original draft, Writing – review & editing. **Antonio García-Casco:** Conceptualization, Investigation, Methodology, Supervision, Validation, Visualization, Writing – review & editing.

## Declaration of competing interest

The authors declare that they have no known competing financial interests or personal relationships that could have appeared to influence the work reported in this paper.

## Acknowledgements

Zeynab Gharamohammadi, Ali Kananian, Philippe Agard and Jafar Omrani are acknowledged for logistical assistance. Olga Cazalla, Laura Crespo and Miguel Angel Hidalgo Laguna are acknowledged for their technical support at Centre of Scientific Instrumentation, University of Granada. We are very grateful to Sophie Nowak for further support during XRD analytical sessions. Onno Oncken is warmly thanked for insightful discussions and support regarding mechanical earthquake-related processes. Hugues Raimbourg and Isabelle Martinez are also acknowledged for exciting discussions and suggestions regarding fluid-rock interaction processes. The editorial handling by Alexander Webb is very much appreciated. Whitney Behr and Volker Schenk are warmly acknowledged for detailed and constructive reviews, but also for their stimulating words that helped improving this work. This project has been funded by an Initiative D'EXcellence (IDEX) grant 16C538 and the TelluS Program of CNRS/INSU to S.A. Partial funding was also provided by the University of Granada at CIC.

## Appendix A. Supplementary material

Supplementary material related to this article can be found online at <https://doi.org/10.1016/j.epsl.2021.117135>.

## References

- Abercrombie, R., Poli, P., Bannister, S., 2017. Earthquake directivity, orientation, and stress drop within the subducting plate at the Hikurangi Margin, New Zealand. *J. Geophys. Res., Solid Earth* 122 (12), 10–176.
- Agard, P., Monié, P., Gerber, W., Omrani, J., Molinaro, M., Meyer, B., Labrousse, L., Vrielynck, B., Jolivet, L., Yamato, P., 2006. Transient, synobduction exhumation of Zagros blueschists inferred from P-T, deformation, time, and kinematic constraints: implications for Neotethyan wedge dynamics. *J. Geophys. Res., Solid Earth* 111 (B11).
- Angiboust, S., Petteke, T., De Hoog, J., Caron, B., Oncken, O., 2014. Channelized fluid flow and eclogite-facies metasomatism along the subduction shear zone. *J. Petrol.* 55 (5), 883–916.
- Angiboust, S., Kirsch, J., Oncken, O., Glodny, J., Monié, P., Rybacki, E., 2015. Probing the transition between seismically coupled and decoupled segments along an ancient subduction interface. *Geochem. Geophys. Geosyst.* 16 (6), 1905–1922.
- Angiboust, S., Agard, P., Glodny, J., Omrani, J., Oncken, O., 2016. Zagros blueschists: episodic underplating and long-lived cooling of a subduction zone. *Earth Planet. Sci. Lett.* 443, 48–58.
- Austrheim, H., Andersen, T., 2004. Pseudotachylytes from Corsica: fossil earthquakes from a subduction complex. *Terra Nova* 16 (4), 193–197.
- Barklage, M., Wiens, D., Conder, J., Pozgay, S., Shiohara, H., Sugioka, H., 2015. P and S velocity tomography of the Mariana subduction system from a combined land-sea seismic deployment. *Geochem. Geophys. Geosyst.* 16 (3), 681–704.
- Behr, W., Platt, J., 2013. Rheological evolution of a Mediterranean subduction complex. *J. Struct. Geol.* 54, 136–155.
- Bird, P., 1978. Stress and temperature in subduction shear zones: Tonga and Mariana. *Geophys. J. Int.* 55 (2), 411–434.
- Bonnet, G., Agard, P., Angiboust, S., Fournier, M., Omrani, J., 2019. No large earthquakes in fully exposed subducted seamount. *Geology* 47 (5), 407–410.
- Bonnet, G., Agard, P., Whitechurch, H., Fournier, M., Angiboust, S., Caron, B., Omrani, J., 2020. Fossil seamount in southeast Zagros records intraoceanic arc to back-arc transition: new constraints for the evolution of the Neotethys. *Gondwana Res.* 81, 423–444.
- Collettini, C., Niemeijer, A., Viti, C., Marone, C., 2009. Fault zone fabric and fault weakness. *Nature* 462 (7275), 907–910.

- Cloos, M., 1986. Blueschists in the Franciscan complex of California: petrotextonic constraints on uplift mechanisms. In: *Blueschists and Eclogites*, vol. 164. Geological Society of America Memoir, pp. 77–93.
- Cox, S., 2010. The application of failure mode diagrams for exploring the roles of fluid pressure and stress states in controlling styles of fracture-controlled permeability enhancement in faults and shear zones. *Geofluids* 10 (1–2), 217–233.
- Delaloye, M., Desmons, J., 1980. Ophiolites and mélange terranes in Iran: a geochronological study and its paleotectonic implications. *Tectonophysics* 68 (1–2), 83–111.
- Dielforder, A., Hetzel, R., Oncken, O., 2020. Megathrust shear force controls mountain height at convergent plate margins. *Nature* 582 (7811), 225–229.
- Di Toro, G., Pennacchioni, G., Nielsen, S., 2009. Pseudotachylytes and earthquake source mechanics. *Int. Geophys.* 94, 87–133.
- Eimer, M., Wiens, D., Cai, C., Lizzaralde, D., Jasperson, H., 2020. Seismicity of the incoming plate and forearc near the Mariana Trench recorded by ocean bottom seismographs. *Geochem. Geophys. Geosyst.* 21 (4), e2020GC008953.
- Emry, E., Wiens, D., Shiobara, H., Sugioka, H., 2011. Seismogenic characteristics of the Northern Mariana shallow thrust zone from local array data. *Geochem. Geophys. Geosyst.* 12 (12).
- Evans, B.W., 1990. Phase relations of epidote-blueschists. *Lithos* 25 (1–3), 3–23.
- Fagereng, Å., Diener, J., Ellis, S., Remitti, F., 2018. Fluid-Related Deformation Processes at the up-and down-Dip Limits of the Subduction Thrust Seismogenic Zone: What do the Rocks Tell Us, vol. 534. *Geol. Soc. Am. Spec. Pap.*, p. 1.
- Frank, W., Shapiro, N., Husker, A., Kostoglodov, V., Bhat, H., Campillo, M., 2015. Along-fault pore-pressure evolution during a slow-slip event in Guerrero, Mexico. *Earth Planet. Sci. Lett.* 413, 135–143.
- Fryer, P., et al., 2020. Mariana serpentinite mud volcanism exhumes subducted seamount materials: implications for the origin of life. *Philos. Trans. R. Soc. Lond. A* 378 (2165), 20180425.
- Gao, J., John, T., Klemd, R., Xiong, X., 2007. Mobilization of Ti–Nb–Ta during subduction: evidence from rutile-bearing dehydration segregations and veins hosted in eclogite, Tianshan, NW China. *Geochim. Cosmochim. Acta* 71 (20), 4974–4996.
- Grove, M., Bebout, G.E., 1995. Cretaceous tectonic evolution of coastal southern California: insights from the Catalina Schist. *Tectonics* 14 (6), 1290–1308.
- Hyndman, R., Yamano, M., Oleskevich, D., 1997. The seismogenic zone of subduction thrust faults. *Isl. Arc* 6 (3), 244–260.
- John, T., Schenk, V., 2006. Interrelations between intermediate-depth earthquakes and fluid flow within subducting oceanic plates: constraints from eclogite facies pseudotachylytes. *Geology* 34 (7), 557–560.
- Kay, M., Main, I., Elphick, S., Ngwenya, B., 2006. Fault gouge diagenesis at shallow burial depth: solution-precipitation reactions in well-sorted and poorly sorted powders of crushed sandstone. *Earth Planet. Sci. Lett.* 243 (3–4), 607–614.
- Lin, A., 2007. *Fossil Earthquakes: The Formation and Preservation of Pseudotachylytes*, vol. 111. Springer.
- Lin, A., 2011. Seismic slip recorded by fluidized ultracataclastic veins formed in a coseismic shear zone during the 2008 Mw 7.9 Wenchuan earthquake. *Geology* 39 (6), 547–550.
- Maekawa, H., Shozul, M., Ishii, T., Fryer, P., Pearce, J., 1993. Blueschist metamorphism in an active subduction zone. *Nature* 364 (6437), 520–523.
- Maekawa, H., Yamamoto, K., Ueno, T., Osada, Y., Nogami, N., 2004. Significance of serpentinites and related rocks in the high-pressure metamorphic terranes, circum-Pacific regions. *Int. Geol. Rev.* 46 (5), 426–444.
- Magloughlin, J., Spray, J., 1992. Frictional melting processes and products in geological materials: introduction and discussion. *Tectonophysics* 204 (3–4), 197–204.
- Menant, A., Angiboust, S., Monie, P., Oncken, O., Guigner, J., 2018. Brittle deformation during Alpine basal accretion and the origin of seismicity nests above the subduction interface. *Earth Planet. Sci. Lett.* 487, 84–93.
- Meneghini, F., Di Toro, G., Rowe, C., Moore, J., Tsutsumi, A., Yamaguchi, A., 2010. Record of mega-earthquakes in subduction thrusts: the black fault rocks of Pasagshak point (Kodiak Island, Alaska). *Geol. Soc. Am. Bull.* 122 (7–8), 1280–1297.
- Moore, D., Lockner, D., Ma, S., Summers, R., Byerlee, J., 1997. Strengths of serpentinite gouges at elevated temperatures. *J. Geophys. Res., Solid Earth* 102 (B7), 14787–14801.
- Muñoz-Montecinos, J., Angiboust, S., Cambeses, A., García-Casco, A., 2020. Multiple veining in a paleo-accretionary wedge: the metamorphic rock record of prograde dehydration and transient high pore-fluid pressures along the subduction interface (Western series, central Chile). *Geosphere* 16 (3), 765–786.
- Muñoz-Montecinos, J., Angiboust, S., García-Casco, A., Glodny, J., Bebout, G., 2021. Episodic hydrofracturing and large-scale flushing along deep subduction interfaces: implications for fluid transfer and carbon recycling (Zagros Orogen, south-eastern Iran). *Chem. Geol.* 120173.
- Oakley, A., Taylor, B., Moore, G., 2008. Pacific plate subduction beneath the central Mariana and Izu-Bonin fore arcs: new insights from an old margin. *Geochem. Geophys. Geosyst.* 9 (6).
- Proctor, B., Mitchell, T., Hirth, G., Goldsby, D., Zorzi, F., Platt, J., Di Toro, G., 2014. Dynamic weakening of serpentinite gouges and bare surfaces at seismic slip rates. *J. Geophys. Res., Solid Earth* 119 (11), 8107–8131.
- Reinen, L., 2000. Seismic and aseismic slip indicators in serpentinite gouge. *Geology* 28 (2), 135–138.
- Rice, J., 2006. Heating and weakening of faults during earthquake slip. *J. Geophys. Res., Solid Earth* 111 (B5).
- Rowe, C., Moore, J., Meneghini, F., McKeirnan, A., 2005. Large-scale pseudotachylytes and fluidized cataclases from an ancient subduction thrust fault. *Geology* 33 (12), 937–940.
- Rowe, C., Griffith, W., 2015. Do faults preserve a record of seismic slip: a second opinion. *J. Struct. Geol.* 78, 1–26.
- Sabzehei, M.S., 1974. *Les melange ophiolitiques de la region d'Esfandagheh*. These d'etate, Université Scientifique et Médicale de Grenoble.
- Scholz, C., Campos, J., 2012. The seismic coupling of subduction zones revisited. *J. Geophys. Res., Solid Earth* 117 (B5).
- Sibson, R.H., 1989. Earthquake faulting as a structural process. *J. Struct. Geol.* 11 (1–2), 1–14.
- Sibson, R., Toy, V., 2006. The habitat of fault-generated pseudotachylyte: presence vs. absence of friction-melt. In: Abercrombie, eds R., McGarr, A., Di Toro, G., Kanamori, H. (Eds.), *Earthquakes: Radiated Energy and the Physics of Faulting*.
- Sibson, R., 2013. Stress switching in subduction forearcs: implications for overpressure containment and strength cycling on megathrusts. *Tectonophysics* 600, 142–152.
- Tamblyn, R., Zack, T., Schmitt, A., Hand, M., Kelsey, D., Morrissey, L., Pabst, S., Savov, I., 2019. Blueschist from the Mariana forearc records long-lived residence of material in the subduction channel. *Earth Planet. Sci. Lett.* 519, 171–181.
- Tarling, M., Smith, S., Viti, C., Scott, J., 2018. Dynamic earthquake rupture preserved in a creeping serpentinite shear zone. *Nat. Commun.* 9 (1), 1–8.
- Ujii, K., Yamaguchi, A., Kimura, G., Toh, S., 2007. Fluidization of granular material in a subduction thrust at seismogenic depths. *Earth Planet. Sci. Lett.* 259 (3–4), 307–318.
- Ujii, K., Tsutsumi, A., Fialko, Y., Yamaguchi, H., 2009. Experimental investigation of frictional melting of argillite at high slip rates: implications for seismic slip in subduction-accretion complexes. *J. Geophys. Res., Solid Earth* 114 (B4).
- Ujii, K., Ito, K., Nagate, A., Tabata, H., 2021. Frictional melting and thermal fracturing recorded in pelagic sedimentary rocks of the Jurassic accretionary complex, central Japan. *Earth Planet. Sci. Lett.* 554, 116638.
- Wang, K., Huang, T., Tilmann, F., Peacock, S., Lange, D., 2020. Role of serpentinitized mantle wedge in affecting megathrust seismogenic behavior in the area of the 2010Mw=8.8 Maule earthquake. *Geophys. Res. Lett.* 47, e2020GL0482.